Supporting Information for

Trace Level Al^{3+} Detection in Aqueous Media utilizing Luminescent Ensembles Comprising Pyrene Laced Dynamic Surfactant Assembly

Nilanjan Dey, [a] Santanu Bhattacharya, [a, b,*]

[a]Department of Organic Chemistry, Indian Institute of Science, Bangalore 560012, India.

[b]Present Address: Director's Research Unit, Indian Association for Cultivation of Science, Kolkata 700032, India.

*Corresponding author: E-mail: sb@orgchem.iisc.ernet.in

Additional Spectra

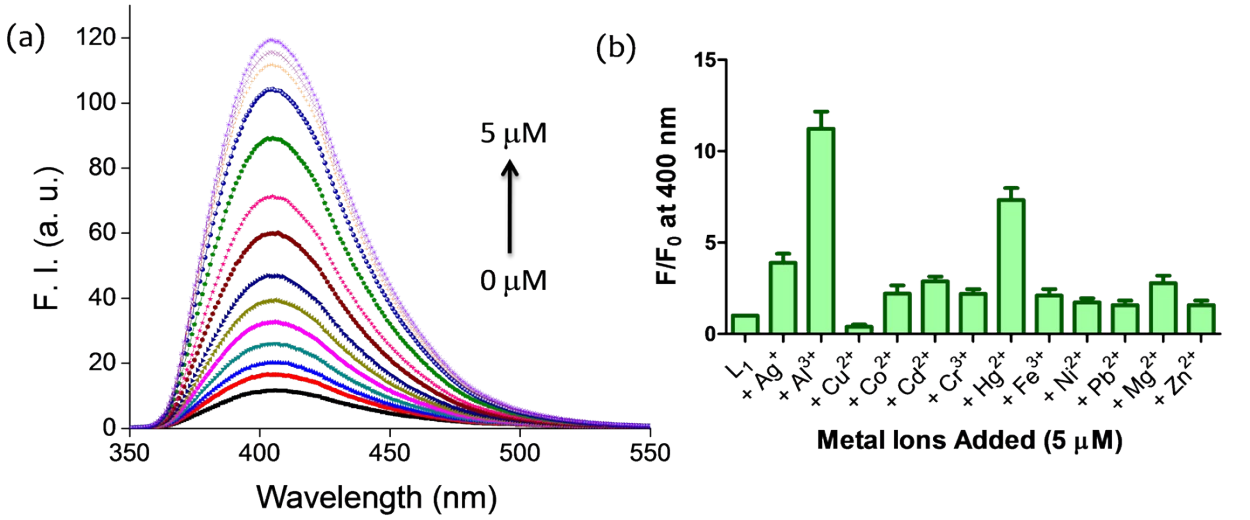

Figure S1. (a) Fluorescence titration of $\mathbf{L_1}$ (10 μM, λex = 340 nm) with Al^{3+} in acetonitrile medium. (b) Change in emission intensity of $\mathbf{L_1}$ (10 μM, λex = 340 nm) at 400 nm upon addition of different metal ions in acetonitrile.

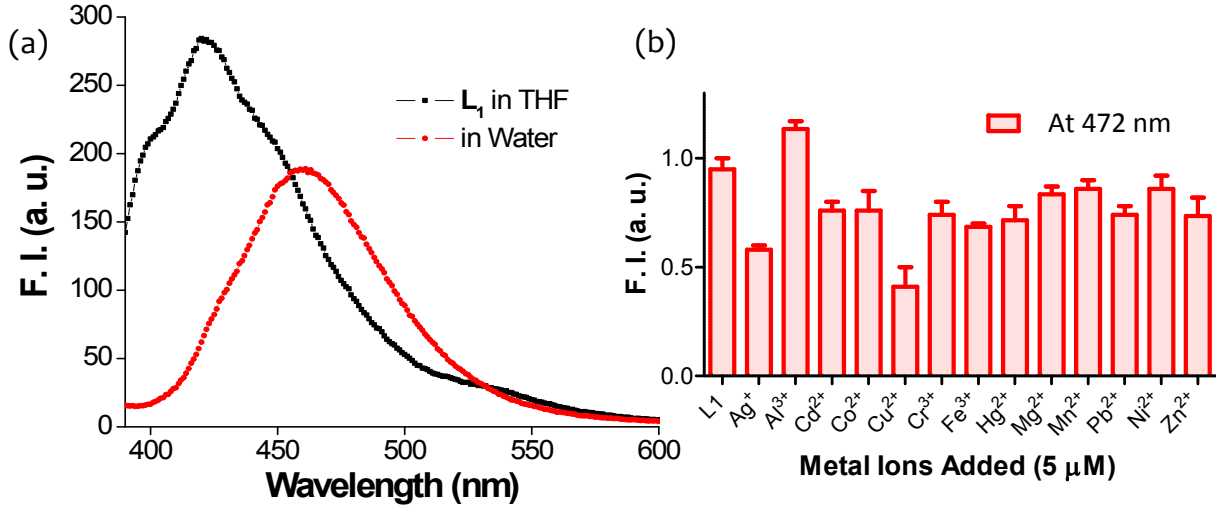

Figure S2. (a) Emission spectra of $\mathbf{L_1}$ (10 μM, λex = 340 nm) in THF and water medium. (b) Change in emission intensity of $\mathbf{L_1}$ (10 μM, λex = 340 nm) at 472 nm upon addition of different metal ions in water.

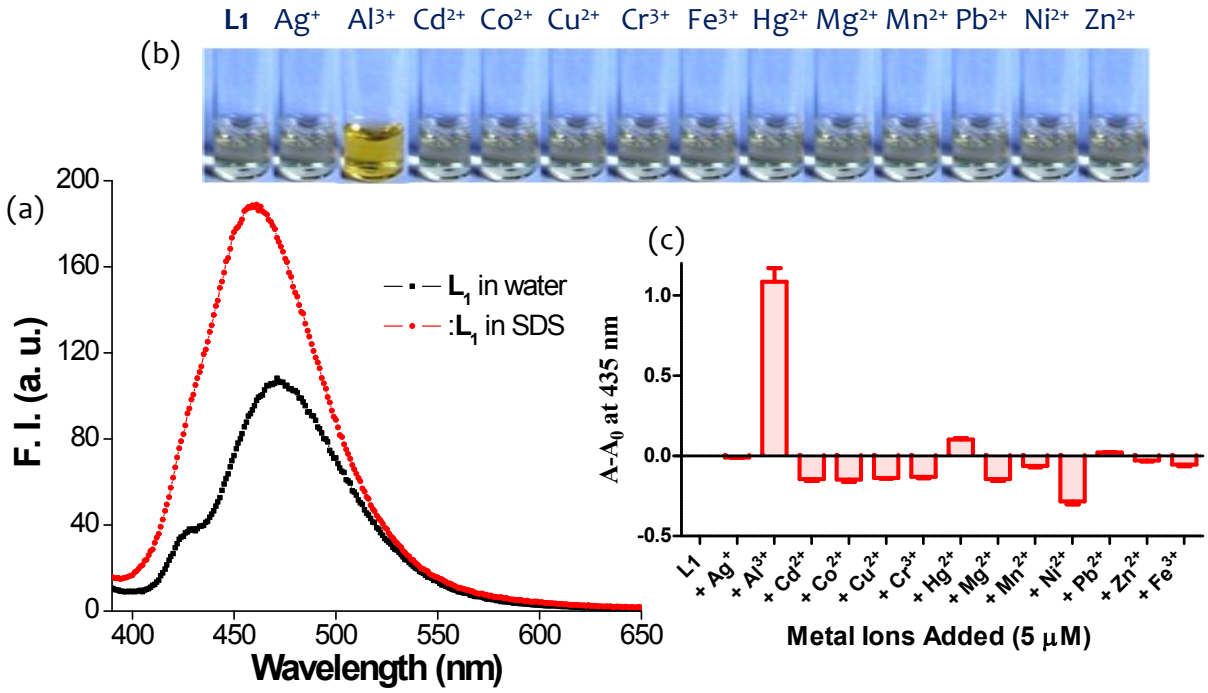

Figure S3. (a) Emission spectra of $\mathbf{L_1}$ (10 μM, λex = 340 nm) in water and SDS (8 mM) medium. (b) Images of compound in presence of different metal ions in SDS medium. (c) Change in absorbance of $\mathbf{L_1}$ (10 μM, λex = 340 nm) at 435 in SDS medium.

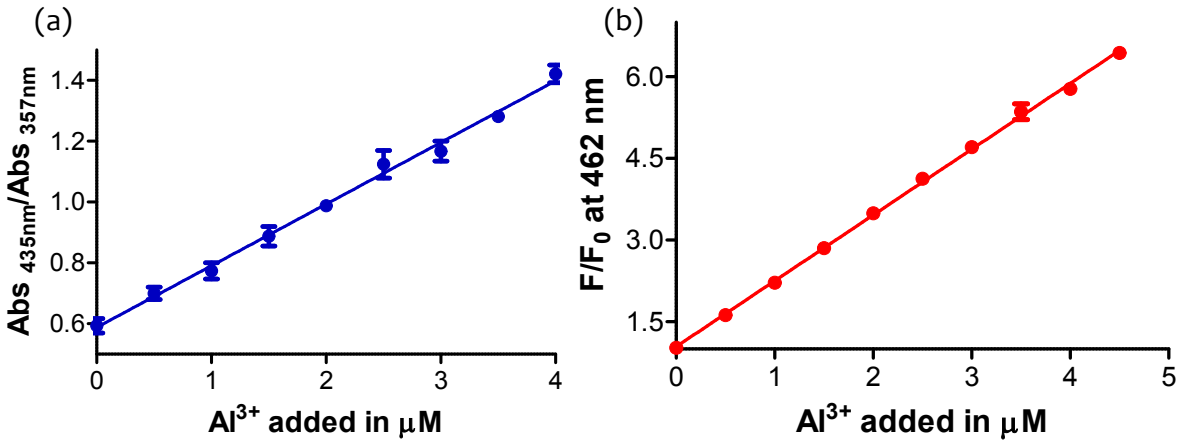

Figure S4. (a) Ratiometric response of $\mathbf{L_1}$ (10 μM) in presence of Al^{3+} in SDS (8 mM) medium. (b) Change in emission intensity of $\mathbf{L_1}$ (10 μM, λex = 340 nm) in presence Al^{3+} in SDS (8 mM) medium.

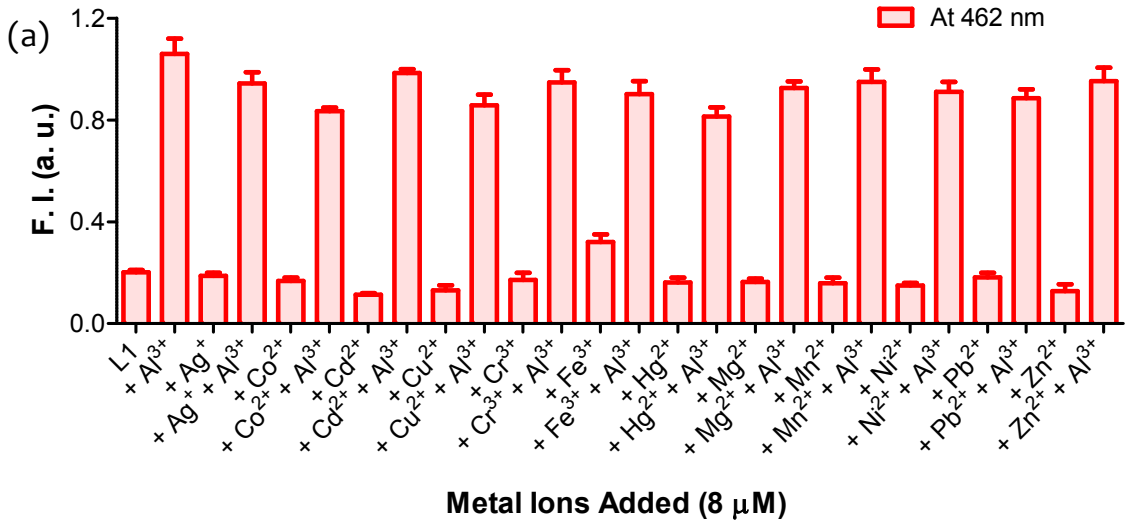

(b)

Medium	Anisotropy
L1 in water	0.087 ± 0.01
L1 in Birj-58	0.102 ± 0.03
L1 in CTAB	0.125 ± 0.07
L1 in SDS	0.167 ± 0.02

Figure S5. (a) Al^{3+} induced change in emission intensity of $\mathbf{L_1}$ (10 μM, λex = 340 nm) in presence of other metal ions (8 μM) SDS (8 mM) medium. (c) Anisotropy values of $\mathbf{L_1}$ in different surfactant medium.

Detail procedure for calculating detection limit

A solution of compound $\mathbf{L_1}$ in SDS micelle medium (8 mM) showed enhancement in the emission intensity at 462 nm band upon addition of Al^{3+} (λex = 340 nm). Therefore

measurements have been carried out at this wavelength for calibration. Overall 7 measures and 10 blank replicates were used for calibration.

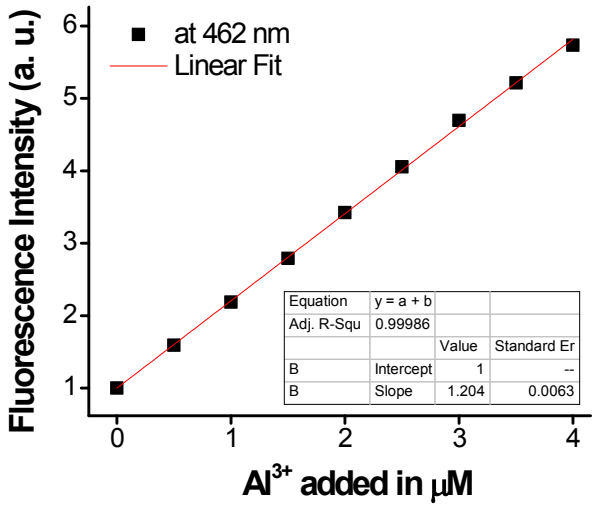

Al^{3+} added µM	F/F_0 at 462 nm
0	1
0.5	1.59
1	2.19
1.5	2.78
2	3.42
2.5	4.05
3	4.69
3.5	5.21
4	5.73

Figure S6. Calibration plot of $\mathbf{L_1}$ with Al^{3+} at 462 nm wavelength

Al^{3+} concentrations were calculated from the equation 1 as obtained from the calibration curve (a straight line) (fig. S6).

$Y = 1.2043x + 1$…….(1)

Then these calculated caffeine concentrations, represented as $[Al^{3+}]$calcd. were plotted against actually added Al^{3+}, represented as $[Al^{3+}]$actual. Slope (b) of this plot (fig. S7) was further used for calculating the detection limit in terms of concentration.

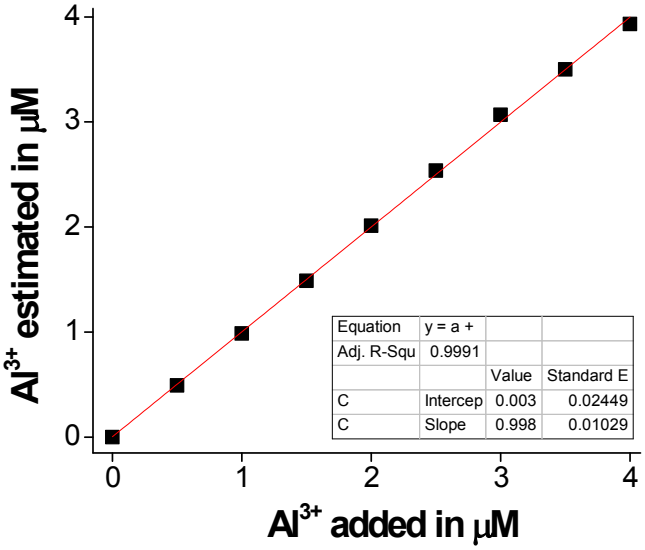

Figure S7. New calibration plot

Thereafter, from the measured blank emission values of $\mathbf{L_1}$ (10 μM, λex = 340 nm), the concentrations of Al^{3+} were calculated using the equation [1].

Replicate	F/F_0 at 462 nm
1	1.012
2	1.034
3	1.022
4	1.013
5	1.035
6	1.025
7	1.022
8	1.031
9	1.028
10	1.026

The mean (x) and the standard deviation (s) from Al^{3+} concentrations as calculated from the blank replicates are,

$(x \pm s) = (0.02018 + 0.00653) \times 10^{-6}$

The decision limit (Lc) was calculated using equation [2].

$L_c = t_c \times s \times (1 + 1/N)^{1/2}$.....[2]

For the probability level of 5%, t_c will be 1.833 for 9 degrees of freedom (GL = N-1 = 10-1 = 9) and N denotes the number of blank replicates.

So, in the present case, considering N = 10, we obtain,

$L_c = 1.833 \times (0.00653 \text{ x } 10^{-6}) \times (1 + 1/10)^{1/2} = 0.01257 \times 10^{-6}$ M

The detection limit (L_D) is considered as the double of the decision limit,

$L_D = 2 \times Lc = 0.0251 \times 10^{-6}$ M

The detection limit (x_D) in concentration term will be

$x_D = 2x_c = 2\ L_c/b = (0.0251 \times 10^{-6})/0.99915 = 0.02516 \times 10^{-6}$ M

Thus, the detection limit for caffeine is obtained as 0.025 μM or 5.36 ppb.

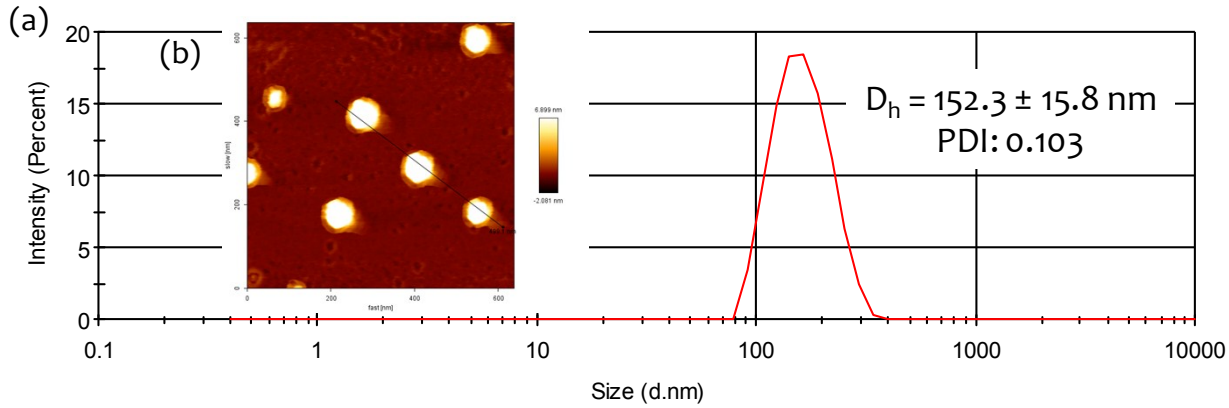

Figure S8. (a) Hydrodynamic diameter of $\mathbf{L_1}$ doped SoyPC vesicle in water. (b) AFM images of $\mathbf{L_1}$ doped SoyPC vesicle in water.

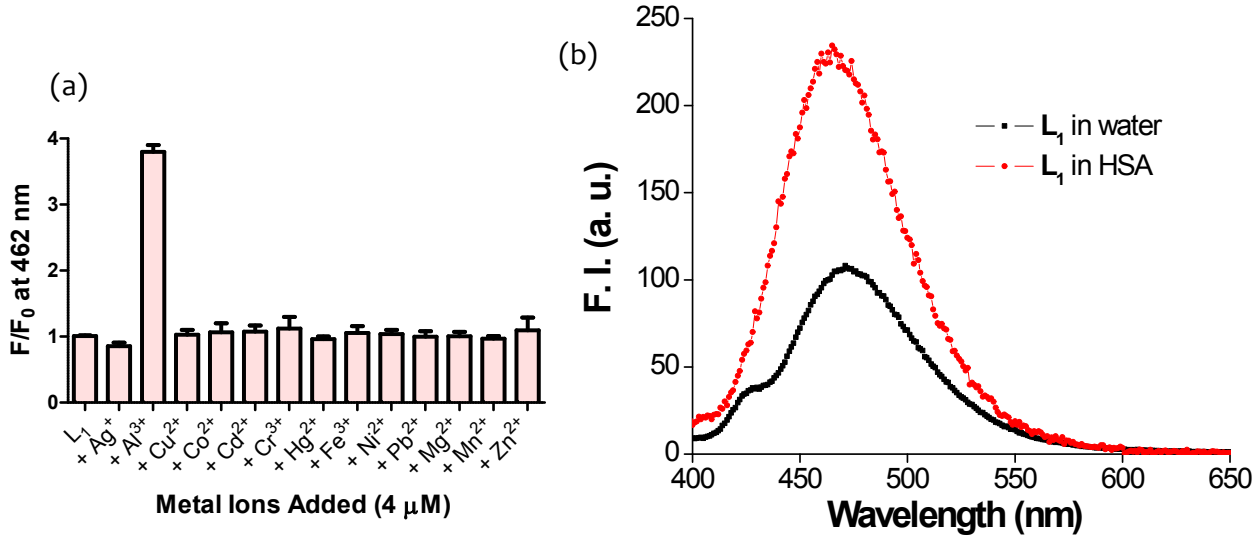

Figure S9. (a) Emission intensity of $\mathbf{L_1}$ doped SoyPC (10 μM, λex = 340 nm) with different metal ions in water. (b) Emission spectra of $\mathbf{L_1}$ (10 μM, λex = 340 nm) in water and in presence of HSA.

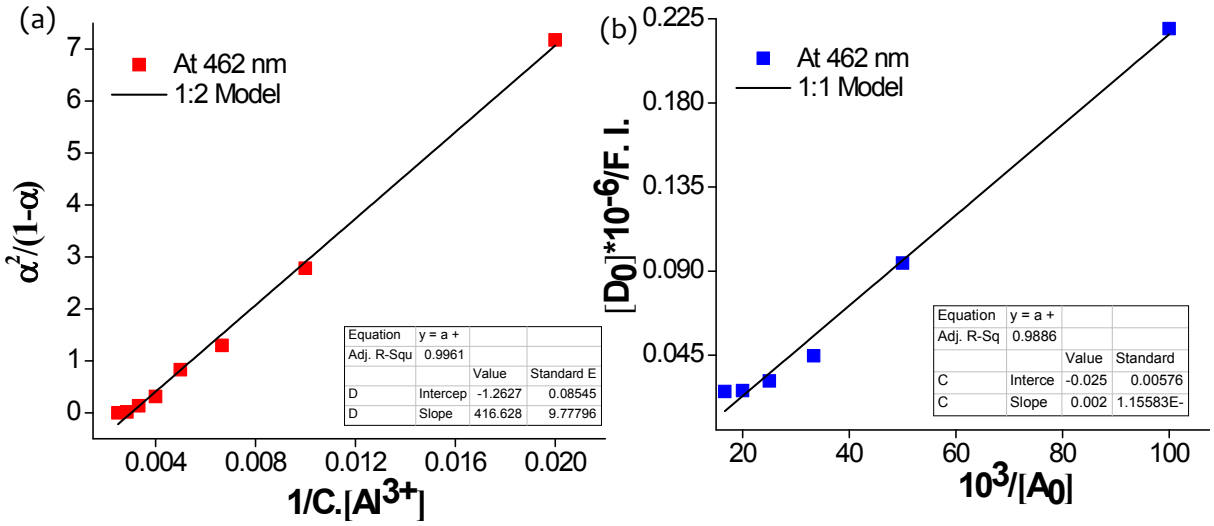

Figure S10. (a) Determination of binding constant $\mathbf{L_1}$ (10 μM, λex = 340 nm) with Al^{3+} in SDS medium. (b) Determination of binding constant $\mathbf{L_3}$ (10 μM, λex = 340 nm) with Al^{3+} in SDS medium.

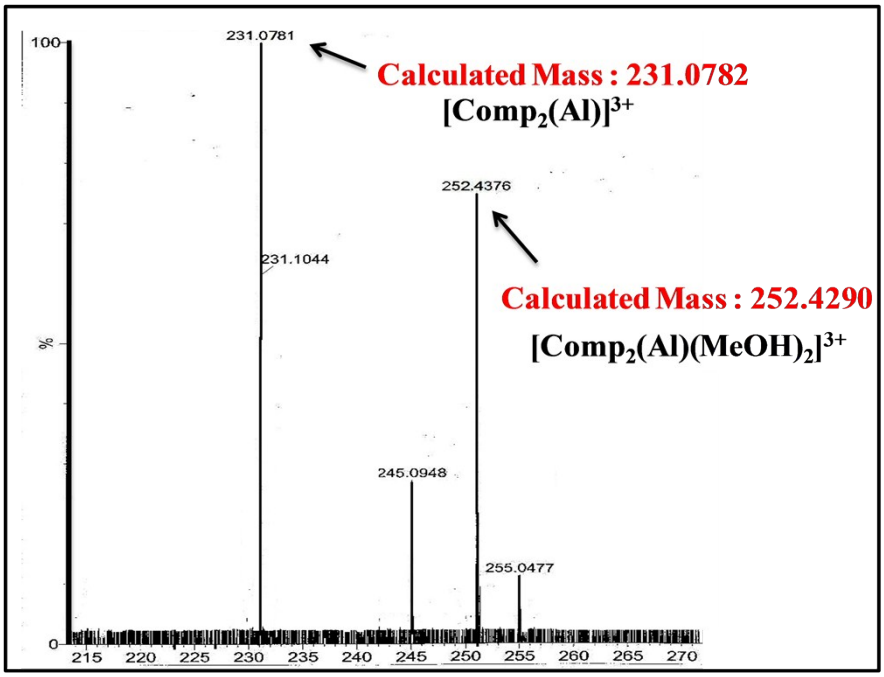

Figure S11. ESI-MS mass spectrum of $\mathbf{L_1}$ in presence of Al^{3+} in SDS medium.

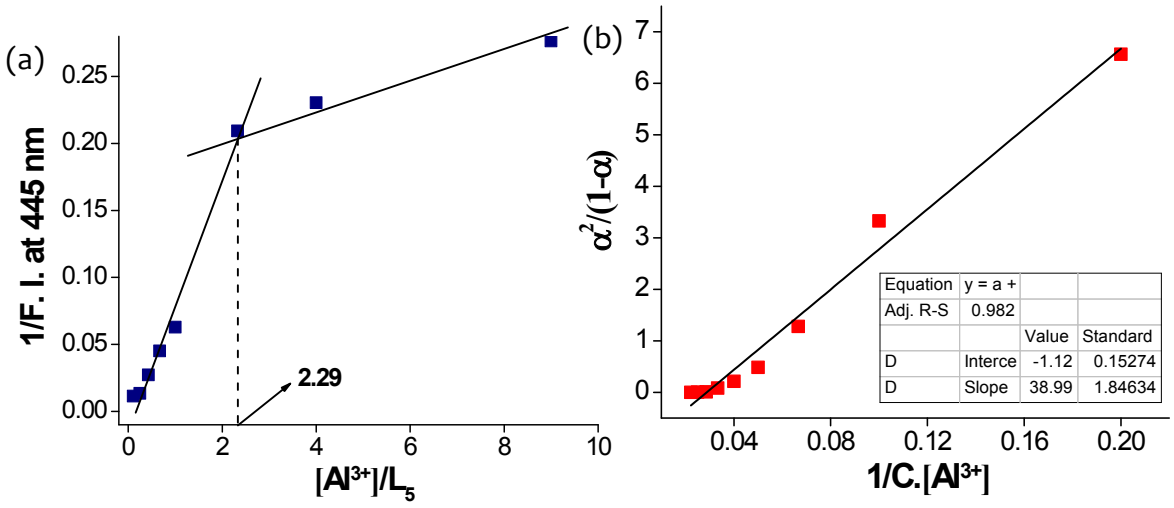

Figure S12. (a) Job plot analyses of $\mathbf{L_5}$ demonstrating 2:1 binding with the Al^{3+} ion. (b) Binding constant was calculated with Al^{3+} ion using Benesi-Hildebrand equation for the 2:1 stoichiometry.

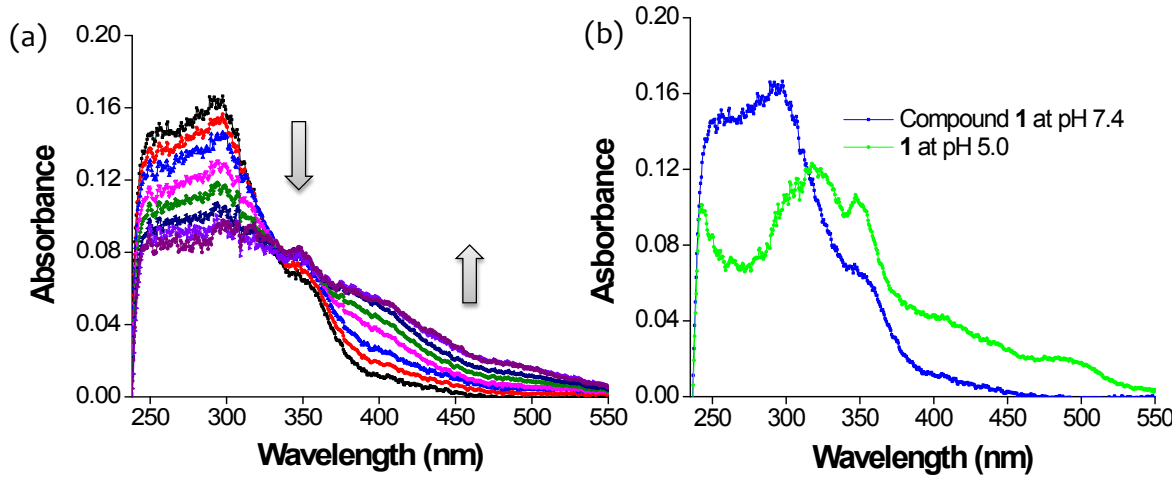

Figure S13. (a) UV-visible spectra of $\mathbf{L_1}$ (10 μM) with SDS (0-1.2 mM) in water medium. (b) UV-visible spectra of $\mathbf{L_1}$ (10 μM) in different buffer medium (7.4 and 5.0) in water.

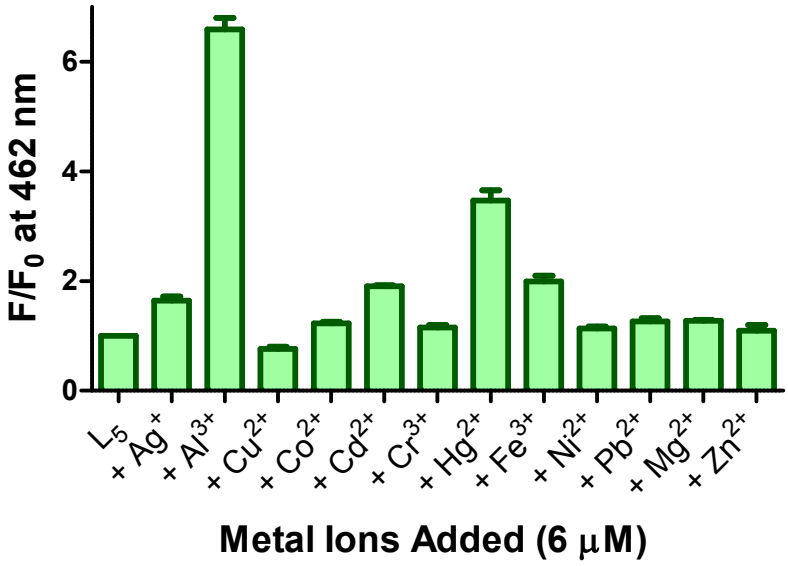

Figure S14. Change in emission intensity of $\mathbf{L_5}$ (10 μM, λex = 340 nm) at 462 nm upon addition of different metal ions in SDS micelle medium (8 mM).

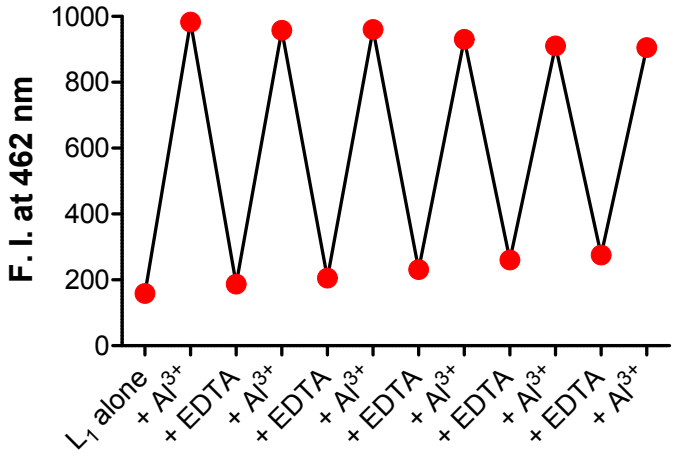

Figure S15. EDTA-mediated recovery experiments with $\mathbf{L_1}$ (10 μM) at 462 nm (5 μM) each time after addition of 5 μM of Al^{3+} in SDS micelle medium (8 mM).

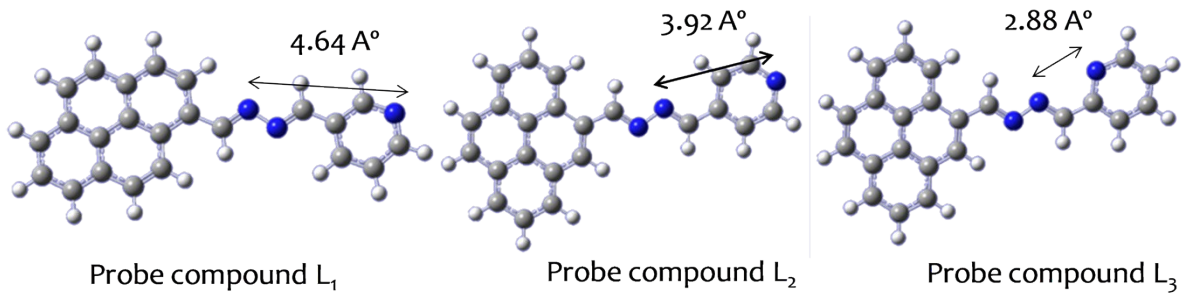

Figure S16. Energy minimized structures of $\mathbf{L_1}$, $\mathbf{L_2}$ and $\mathbf{L_3}$ using B3LYP/6-31G* method.

Probes	Negative charge density on pyridyl nitrogen
$\mathbf{L_1}$	-0.4235
$\mathbf{L_2}$	-0.4123
$\mathbf{L_3}$	-0.3892
$\mathbf{L_4}$	-0.5612

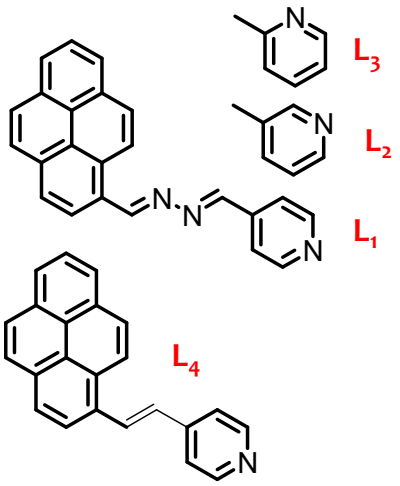

Figure S17. The Mullikan charge distribution on pyridine nitrogen ends of compounds $\mathbf{L_1}$, $\mathbf{L_2}$, $\mathbf{L_3}$ and $\mathbf{L_3}$ using B3LYP/6-31G* method.

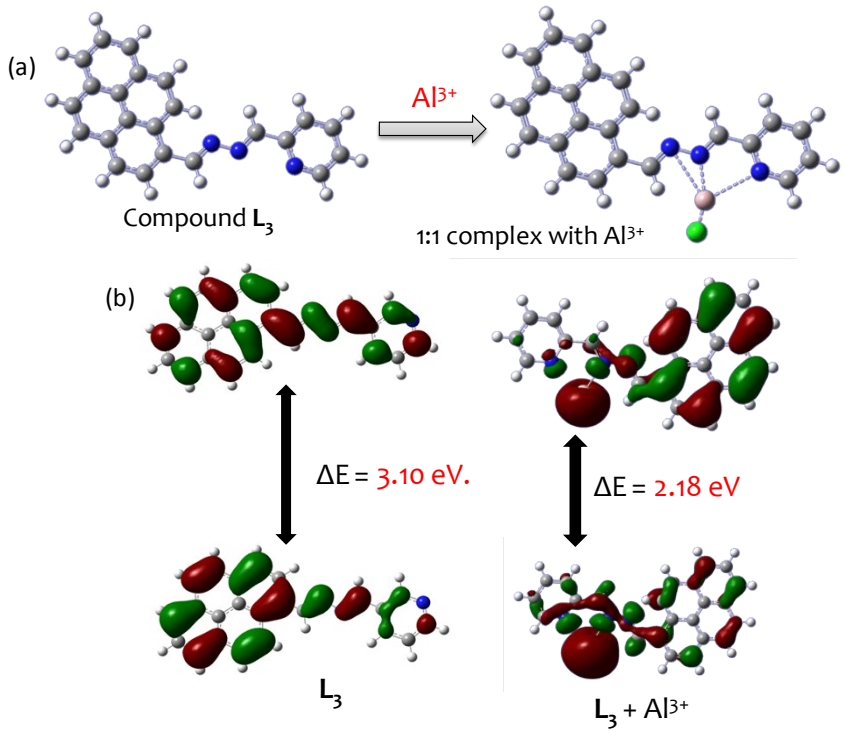

Figure S18. (a) Energy minimized structures of $\mathbf{L_3}$ and $\mathbf{L_3}$ + Al^{3+} using B3LYP/6-31G* method. (b) FMO analysis of $\mathbf{L_3}$ and $\mathbf{L_3}$ + Al^{3+} using B3LYP/6-31G* method.

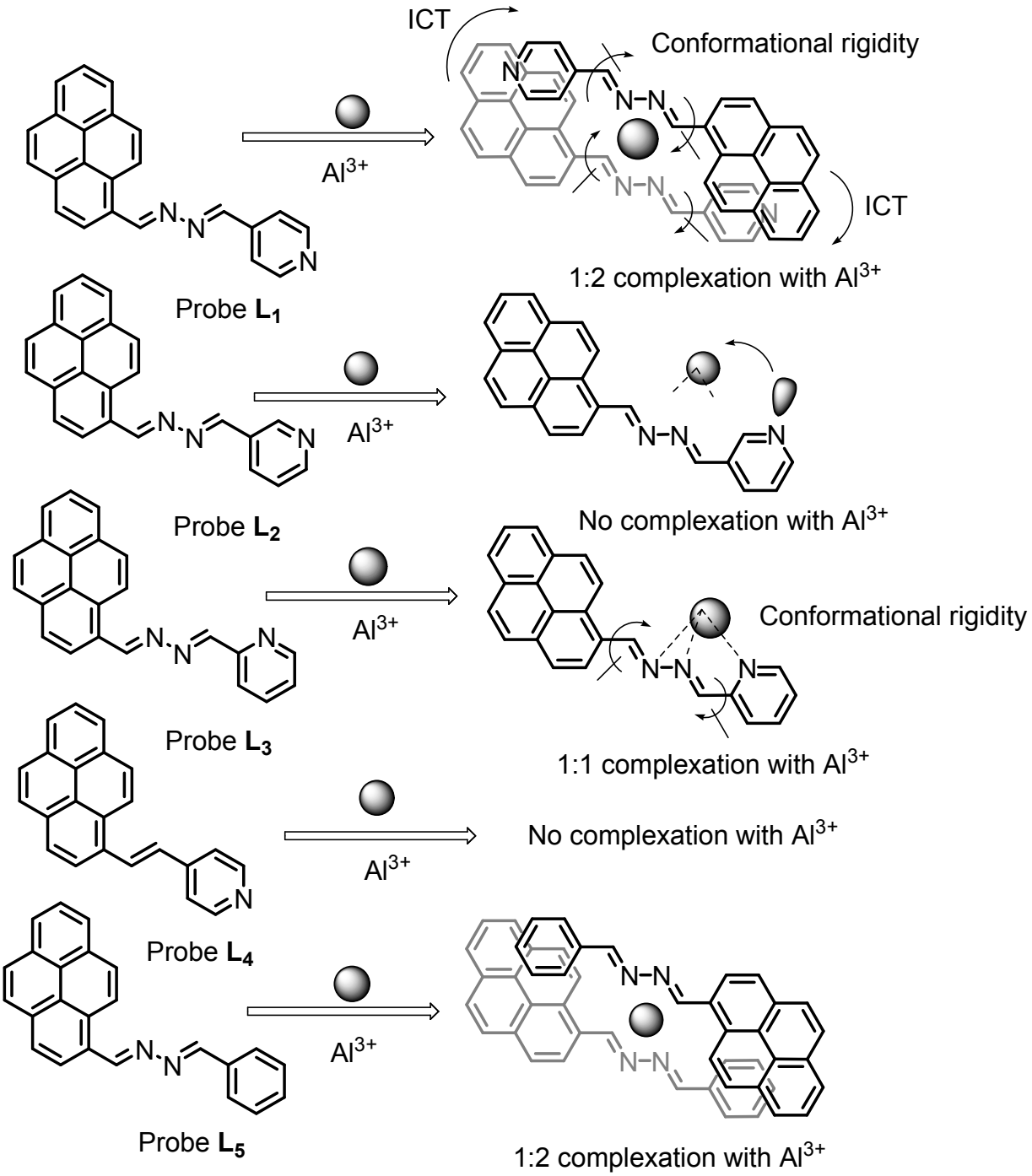
ICT
Conformational rigidity
N
N–N
N–N
N
ICT
Al3+
1:2 complexation with Al3+
Probe L1
Al3+
N–N
N
No complexation with Al3+
Probe L2
Al3+
Conformational rigidity
N–N
N
1:1 complexation with Al3+
Probe L3
No complexation with Al3+
Al3+
N
Probe L4
Al3+
N–N
N–N
1:2 complexation with Al3+
Probe L5

Figure S19. Probable binding modes of compounds $\mathbf{L_1}$ to $\mathbf{L_5}$ with Al^{3+} in SDS micelle medium

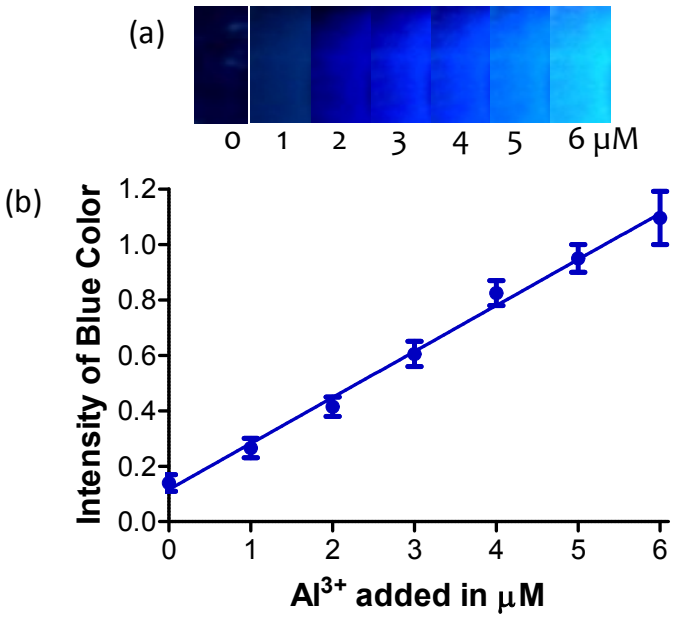

Figure S20. (a) Fluorescence images of $\mathbf{L_1}$ coated TLC plates in presence of different amounts of Al^{3+} (0 – 6 μM). (b) Change in emission intensities of the precoated TLC plates in presence of increasing amount of Al^{3+} (quantified using ImageJ software).

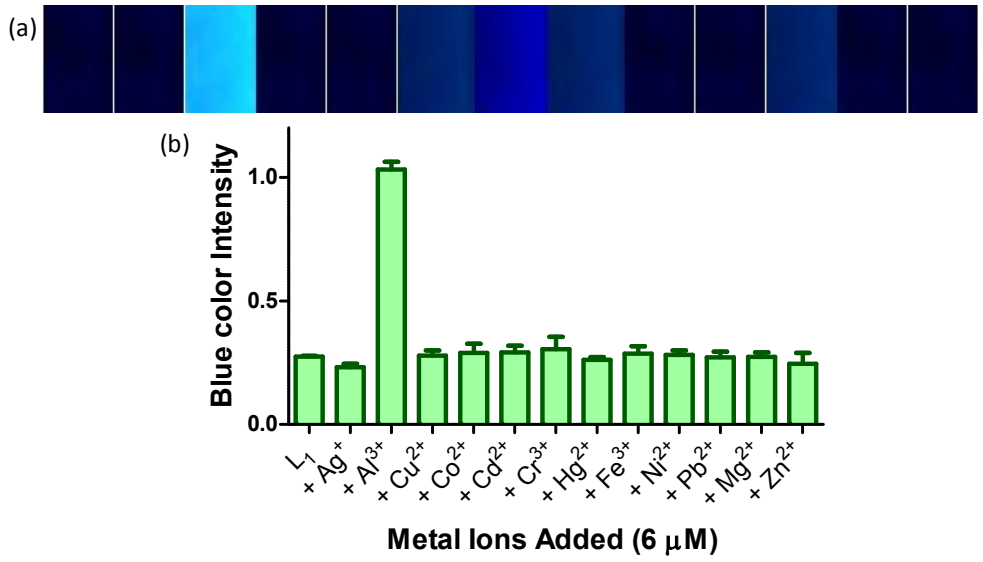

Figure S21. (a) Fluorescence images of $\mathbf{L_1}$ coated TLC plates in presence of different metal ions (6 μM) in water. (b) Change in emission intensities of the precoated TLC plates in presence of different analytes (quantified using ImageJ software).

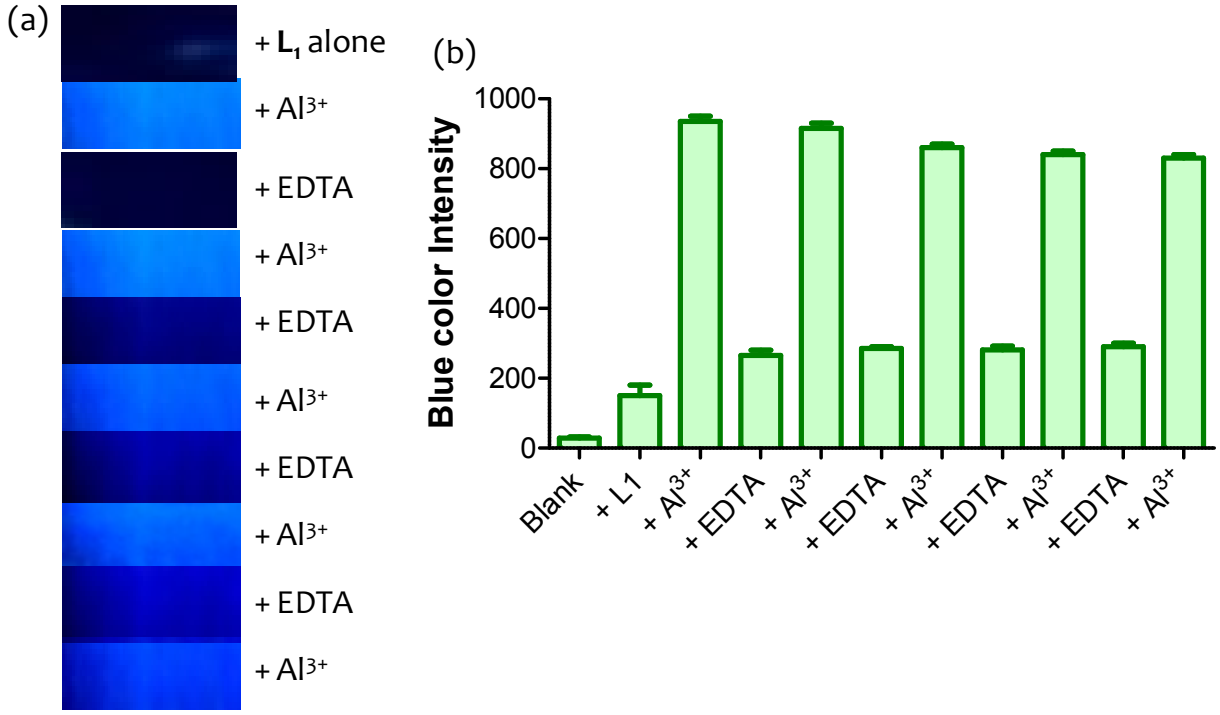

Figure S22. (a) Fluorescence images showing reusability of TLC plates for Al^{3+} sensing. (b) Change in emission intensities of the precoated TLC plates in presence of different analytes (quantified using ImageJ software).

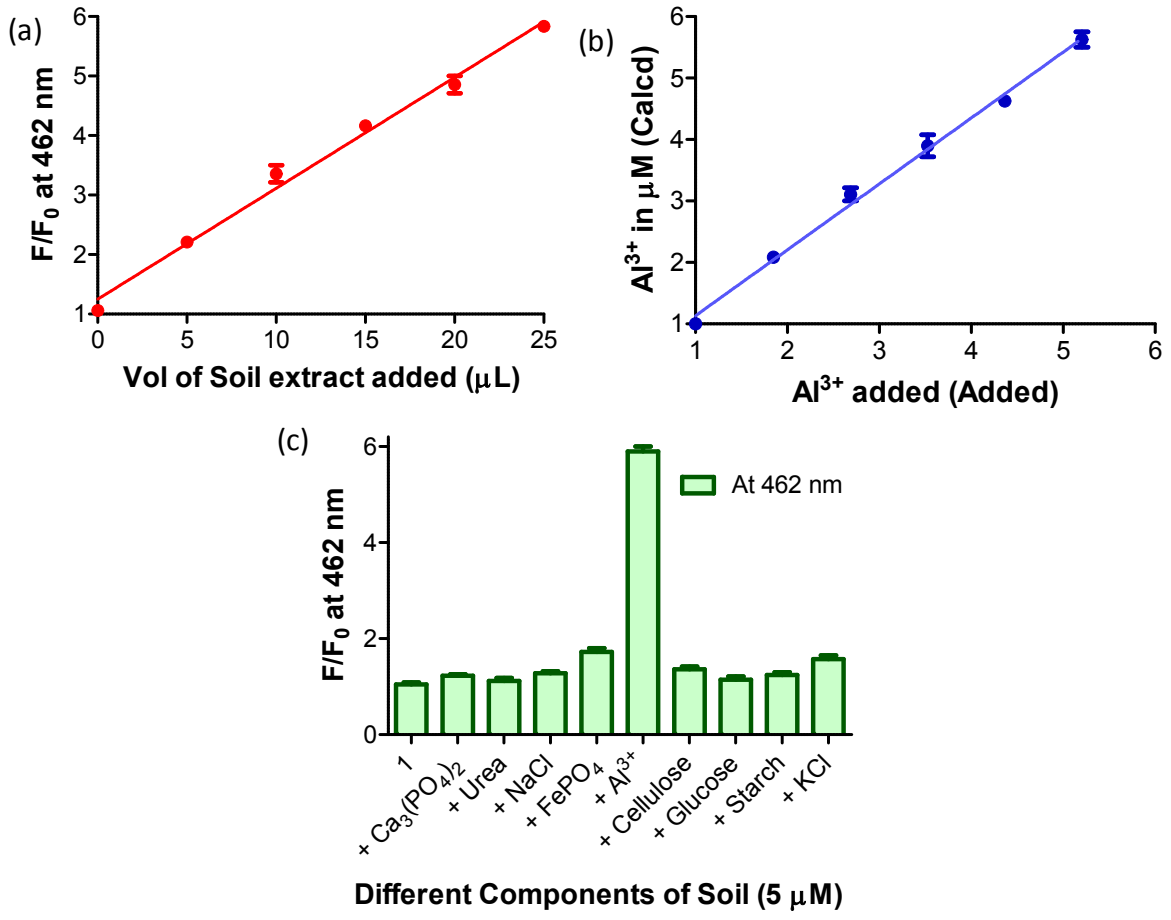

Figure S23. (a) Change in emission intensity of $\mathbf{L_1}$ (10 μM, λex = 340 nm) with Al^{3+}-contaminated soil extract in SDS medium. (b) Recovery plot of $\mathbf{L_1}$ (10 μM, λex = 340 nm) with Al^{3+}-contaminated soil extract in SDS medium. (c) Change in emission intensities of $\mathbf{L_1}$ (10 μM, λex = 340 nm) in presence of different components of soil in SDS medium.

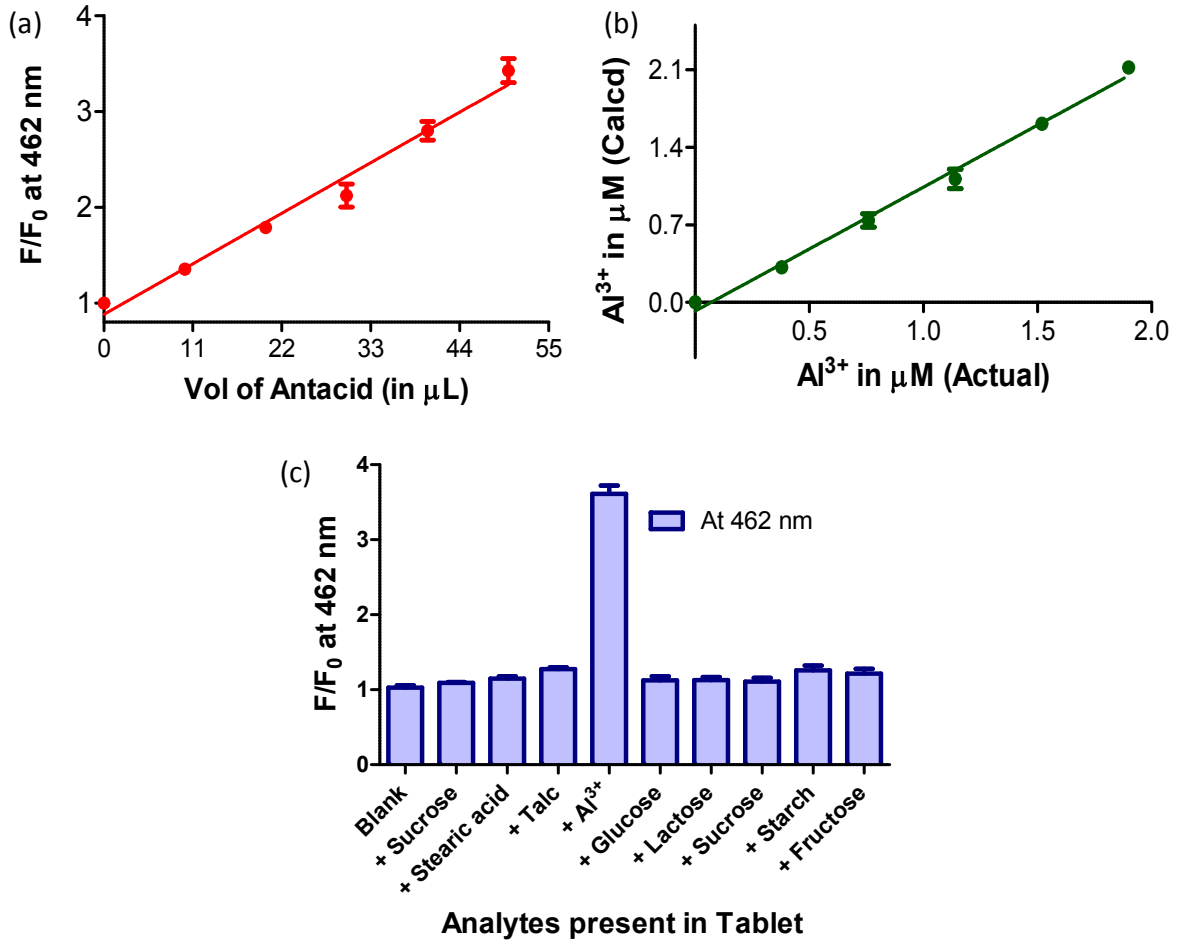

Figure S24. (a) Change in emission intensity of $\mathbf{L_1}$ (10 μM, λex = 340 nm) with aqueous extract of pharmaceutical tablet (Digene) in SDS medium. (b) Recovery plot of $\mathbf{L_1}$ (10 μM, λex = 340 nm) with aqueous extract of pharmaceutical tablet (Digene) in SDS medium. (c) Change in emission intensities of $\mathbf{L_1}$ (10 μM, λex = 340 nm) in presence of different components of Digene in SDS medium.

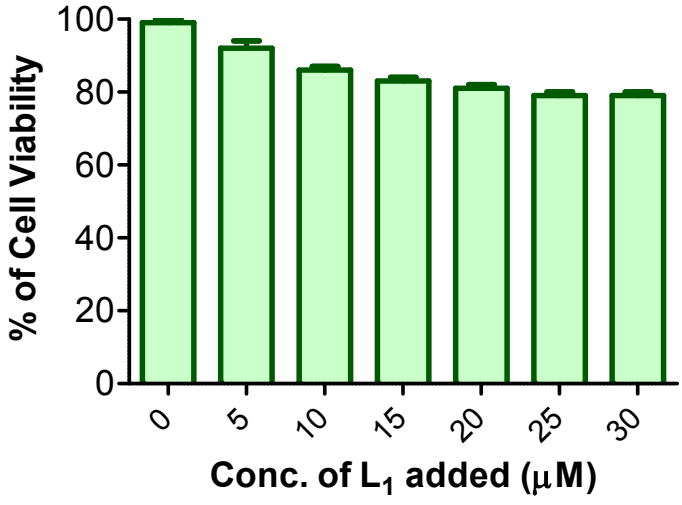

Figure S25. Cell viability assay of compound $\mathbf{L_1}$ in HeLa cells

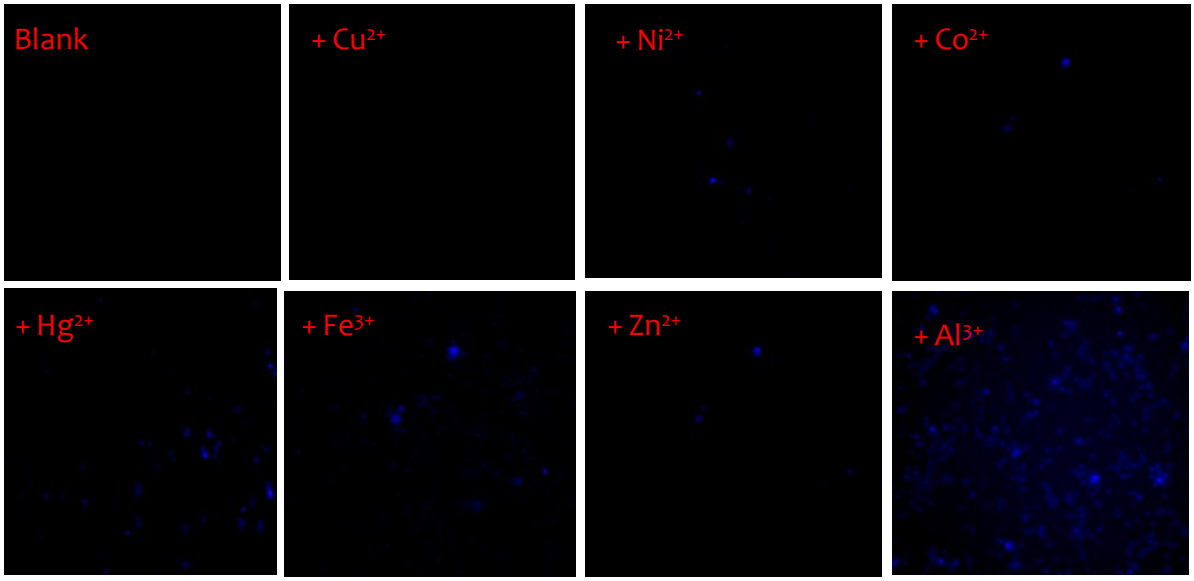

Figure S26. Fluorescent microscopic images of HeLa cells incubated with 10 μM of $\mathbf{L_1}$ in presence and absence of different metal ions (20 μM).

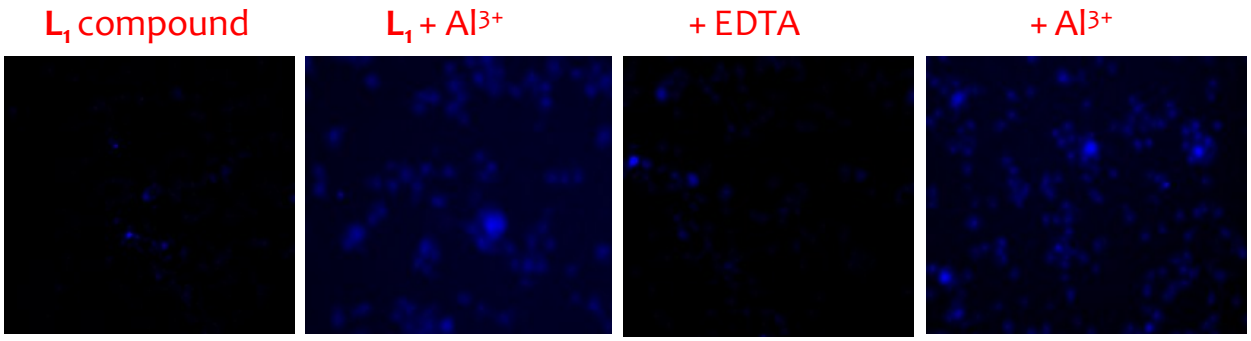

Figure S27. Reversible bioimaging of Al^{3+} (20 μM) in HeLa cells using probe $\mathbf{L_1}$ (10 μM) in presence of chelating agent EDTA (20 μM).

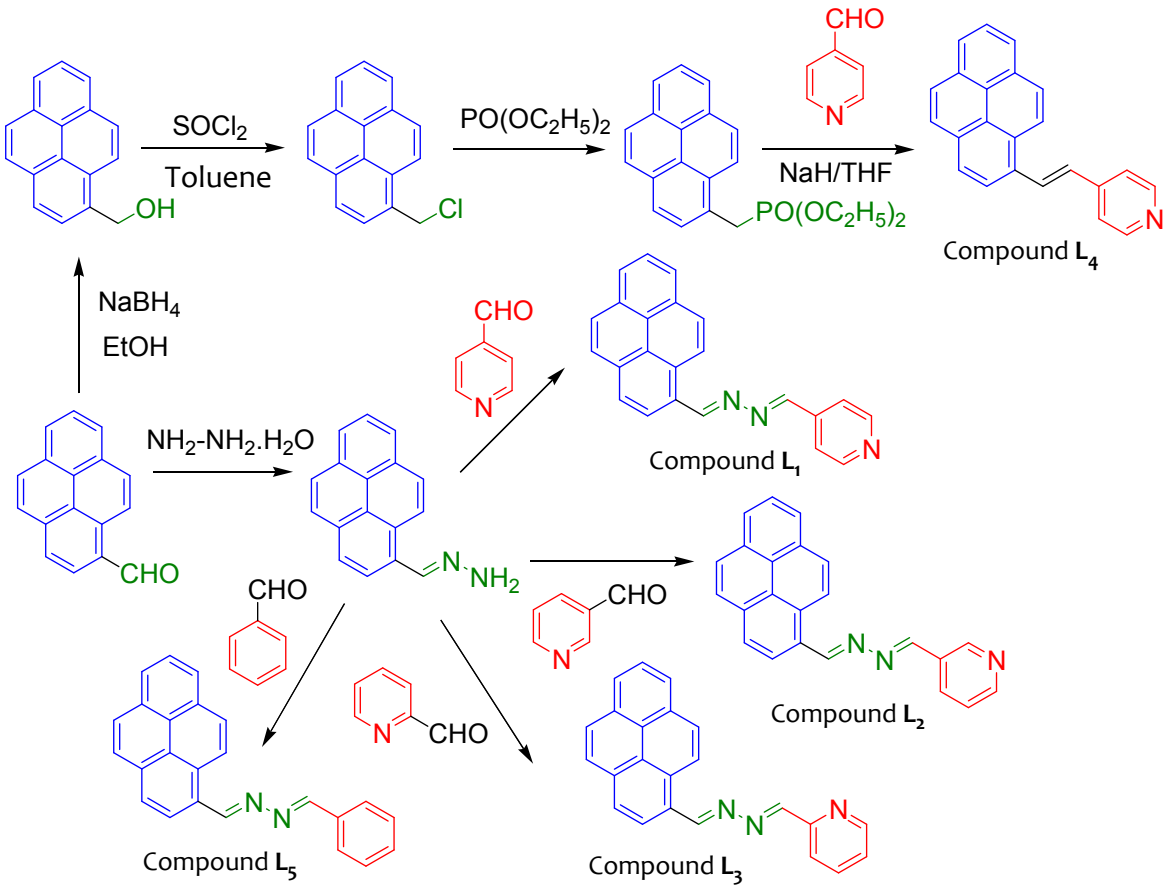

Scheme S1. Synthetic routes to compounds $\mathbf{L_1}$ to $\mathbf{L_5}$

.